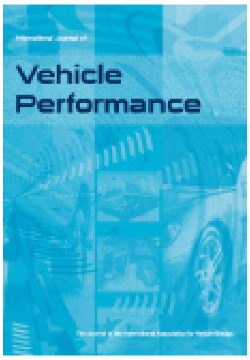

International Journal of Vehicle Performance

ISSN online: 1745-3208 - ISSN print: 1745-3194
https://www.inderscience.com/ijvp

Structural optimisation design of impact resistant composite wheel with compression/injection moulding hybrid structure

Yizhuo Wang, Yingchun Shan, Duo Xu, Xiandong Liu

DOI: 10.1504/IJVP.2024.10060871

Article History:

Received:	22 September 2022
Last revised:	05 February 2023
Accepted:	06 February 2023
Published online:	13 December 2023

Structural optimisation design of impact resistant composite wheel with compression/injection moulding hybrid structure

Yizhuo Wang, Yingchun Shan*, Duo Xu and Xiandong Liu

School of Transportation Science and Engineering,
Beihang University,
South 3rd Street, Gaojiaoyuan, Changping District,
Beijing, 102200, China
Email: 864290541@qq.com
Email: shanych@buaa.edu.cn
Email: 3147543066@qq.com
Email: liuxiandong@buaa.edu.cn
*Corresponding author

Abstract: Based on the advantages of continuous fibre reinforced and long fibre reinforced injection moulding composite wheels, a composite wheel with pressure injection hybrid structure for passenger cars is designed. First, based on the equivalent static load method, the topology of the wheel spokes is optimised under the 13-degree impact dynamics condition, and the initial structure of the wheel is obtained. Then, by analysing the stress state and failure mode under the impact load, the stiffness matching design of the spoke section is carried out to determine the location of the layer and the material ratio. Finally, the parameters of the wheel are optimised, and the final structure of the wheel is obtained. The results show that the optimised wheel can pass the 13-degree impact test, and the weight of the optimised wheel is reduced from 4.61 kg to 3.921 kg.

Keywords: hybrid structure; stiffness matching; impact resistance; optimisation design.

Reference to this paper should be made as follows: Wang, Y., Shan, Y., Xu, D. and Liu, X. (2024) 'Structural optimisation design of impact resistant composite wheel with compression/injection moulding hybrid structure', *Int. J. Vehicle Performance*, Vol. 10, No. 1, pp.1–23.

Biographical notes: Yizhuo Wang is a graduate student in the School of Transportation Science and Engineering of Beihang University. He obtained his Bachelor degree from Beihang University. His main research direction is finite element simulation of automobile tyres and lightweight design of automobiles. He mainly studied the lightweight and parameter optimisation of composite material wheels for central axle type car transporters.

Yingchun Shan is an Associate Professor at the School of Transportation Science and Engineering, Beihang University, China. Her main research interests are automotive structural vibration and noise control, structural signal processing and fault diagnosis, structural strength and lightweight research. She is a member of Chinese Automotive Engineering Association and Beijing Vibration Engineering Association.

Duo Xu is a Post-graduate at the School of Transportation Science and Engineering, Beihang University. He obtained his Bachelor degree from Beihang University. His main research interests are lightweight design of automobiles and research on composite materials. He has mainly studied parameter optimisation of heavy steel wheels, topology optimisation and parameter optimisation of composite wheels, and published two papers in related fields.

Xiandong Liu is a Professor of School of Transportation Science and Engineering, Beihang University, China. His research interests include automotive NVH, fatigue life prediction of automotive components and lightweight design of vehicles. He has published more than 170 papers in domestic and international journals and academic conferences, and co-published a monograph in Elsevier. He won the second prize of National Science and Technology Progress Award in 2003.

1 Introduction

Lightweight is one of the important development trends of automobiles (Miller et al., 2000). As a rotatory unsprung structure, the lightweight wheel can produce better energy-saving (Benedyk, 2000). Composite materials have attracted more and more attention in wheel design due to its excellent properties (Chen, 2011). At present, composite wheels mainly include continuous fibre-reinforced composite wheels and long fibre-reinforced injection moulding composite wheels.

Wheels are the important load-bearing parts in vehicle, which need to meet the corresponding test requirements to ensure safety. Composite wheels are prone to fracture under impact load due to their poor material toughness, so a standard 13-degree impact test is required to verify the impact resistance of the wheels.

At present, many measures have been tried to improve the impact resistance of composite wheels. In 2015, Ford partnered with carbon revolution to equip Shelby GT350R Mustang with carbon wheels, which was the world's first mass-produced carbon wheel. The wheel weighs only 8 kg, while the aluminium alloy wheel of the same specification weighs 15 kg, a weight reduction of nearly 50%. With the progressive application of advanced structure and the resin composition in the wheel, the damage degree of the wheel when hitting the curb at high speed is greatly reduced, and the wheel can pass a series of other rigorous tests (Hua, 2015). In 2014, SABIC and Kringlan composites reported on research to advance the development of the first thermoplastic composite wheel (Grace, 2014). Li et al. (2016) designed a carbon fibre reinforced epoxy resin composite wheel with a specification of 19.5 × 5.5 JJ and a maximum static load of 700kg. The structure was a three-piece type, and the rim and the wheel spoke were layered in one piece with prepreg and formed by an autoclave process. Chang et al. (2010) conducted a 13-degree impact test simulation analysis of a composite wheel with a laminate, and compared the strain of the same part of the same structure. Compared with the aluminium alloy wheel, the strain of the composite wheel is reduced by 30% to 40%. It shows that the impact resistance of composite wheel is better. Bian et al. (2008) simulated and analysed the bending fatigue test of a certain laminated composite wheel. Compared with the aluminium alloy wheel of the same structure, the working stress level is similar, the strength of the composite wheel is higher, and the weight is reduced by 40.74%.

Previous studies have shown that, continuous fibre reinforced composite wheels have excellent impact resistance, but the high cost and long production cycle make it difficult to meet the requirements of mass production of automobiles (Czerwinski, 2021). At present, they are mainly used in sports cars and some expensive passenger cars. Compared with continuous fibre reinforced composite wheels, long fibre reinforced injection moulding composite wheels have the advantages of lower cost, excellent recyclability and short production cycle. However, due to its poorer impact resistance properties, it is difficult for the long fibre reinforced injection moulding composite wheels to pass 13-degree impact test. Batch application in automobiles faces certain challenges.

My research team has carried out a lot of research on long fibre reinforced injection moulded composite wheels. Wan et al. (2015) studied the influence of material anisotropy caused by fibre distribution and orientation on wheel impact response. The results show that the simulation results considering anisotropy are more accurate than those using isotropic material properties. Chai et al. (2018) studied the influence of different material properties on the simulation results of wheel bending fatigue test. In order to obtain the anisotropy of material, a constitutive model was established by spline tension, and then the fibre orientation during injection moulding was simulated. The results show that the results obtained by considering material anisotropy are closer and more accurate than those obtained by isotropic models. Hu et al. (2019) carried out a 13-degree impact test on the wheel. Under the impact load, a penetrating crack occurred in the spoke roots and the wheel could not pass the impact test. The influence of material anisotropy on wheel impact response was also considered. The results show that the simulation results using anisotropic material model are closer to the test results than those using isotropic material model. Aiming at above problems, in this paper, through combining the advantages of the above two kinds of composites materials, the structure of the composite wheel with compression/injection structure is optimised for the impact resistance of a certain type of wheel.

The arrangement of this paper is as follows. Firstly, based on the equivalent static load method, the spoke topology of the wheel is optimised according to the 13-degree impact dynamic condition to obtain the initial structure of the wheel. Then, the stress characteristics and failure modes of the wheels under impact load are analysed, and the stiffness matching design of the spoke section is carried out to determine the position of the layers and the material proportion according to the beam bending model. Finally, the rim and spoke parameters are selected to conduct experimental design, and an approximate model is established to optimise the wheel parameters and obtain the final structure of the wheel.

2 Topology optimisation of long fibre reinforced composite wheels and analysis of simulation results of 13-degree impact test

2.1 13-degree impact test of wheels

GB/T 36581-2018 specifies the method of wheel impact test. The wheel 13-degree impact test device is shown in Figure 1. The steel hammer falls freely in the vertical direction to impact the wheel tyre assembly. The width and length of impact surface of impact hammer are not less than 125 mm and 375 mm respectively. The mass of impact hammer is calculated according to equation (1):

$$m = 0.6W + 180 \tag{1}$$

where m is the hammer mass in kg; W is the maximum static load of the wheel specified by the wheel or vehicle manufacturer in kg.

Figure 1 13-degree impact test bench

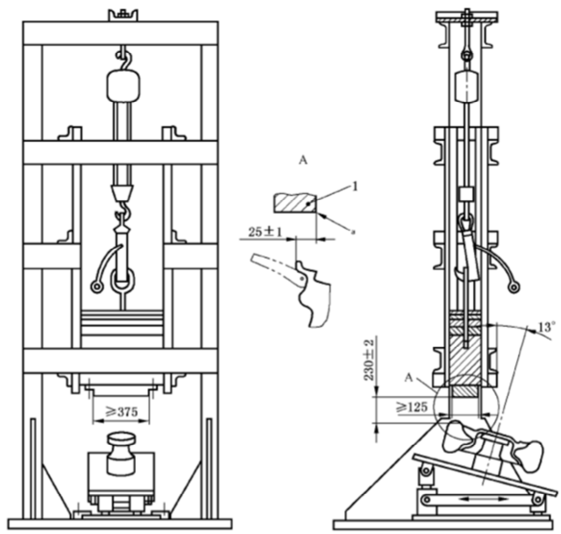

In this paper, a wheel with 15 × 5.5 J size is simulated by 13-degree impact test. Install the wheel and tyre assembly on the test machine, the installation mode should be equivalent to the installation mode of the wheel on the vehicle. Tighten the nuts or bolts to the specified torque value and adjust the position of the wheel so that the angle between the axes and the vertical direction is 13° ± 1°. The rated load of the wheel is 250 kg. According to equation (1), the hammer mass is calculated as 330 kg. The test machine should be calibrated before the test, and the weight of 1,000 kg should be applied to the centre position of the wheel installation along the vertical direction through the calibration connector. The deformation of the central point of the steel beam along the vertical direction under the load should be 7.5 mm±0.75 mm.

If any of the following conditions occur after the test, the test wheel will be determined to be ineffective. Visible cracks penetrate the section of the wheel centre; the centre of the wheel is separated from the rim; the tyre pressure leaks completely within 1 minute. However, if the wheel is deformed or the rim section is broken by impact of a hammer, the test wheel cannot be considered to have failed.

2.2 Wheel topology optimisation under impact conditions based on equivalent static load method

Equivalent static load method as a dynamic structure optimisation method is used here (Kang et al., 2001). The equivalent static load method divides the dynamic process into a certain number of time steps, and each time point can be equivalent to a condition of static analysis. It can generate the same response field as the dynamic and nonlinear analysis at a given time step. By calculating the equivalent static load at each time step through displacement, the dynamic and non-linear responses of the structure can be reproduced under static conditions. In this way, the structure can be statically controlled under multiple working conditions. This method can be applied to structural linear and non-linear dynamic topology, structural non-linear static topology, shape and size optimisation, which have been integrated into commercial software such as HyperWorks.

The wheel topology optimisation is carried out based on HyperWorks, and the wheel topology optimisation model is established in Radioss to minimise the maximum principal strain on the upper surface of wheel spoke. The wheel topology optimisation model is established in Radioss, as shown in Figure 2. In order to save simulation time and improve the efficiency of optimisation, the model is simplified. The bench mainly plays the role of buffering, which will absorb a certain proportion of energy in the impact process, but has little effect on the overall deformation distribution of the wheel. Therefore, the impact bench is removed in the simulation. At the same time, the tyre is removed, and the energy input to the wheel is reduced according to a certain energy proportion. The hammer is assembled to the position where the impact with the rim is about to occur, the falling process of the hammer is omitted, and the hammer is given an initial velocity. The initial velocity v of the hammer is calculated according to equation (2).

$$v = \sqrt{2gh(1-\eta)} \tag{2}$$

where v is the initial speed of the hammer; g is gravity acceleration; h is the drop height of hammer; η is the proportion of energy absorbed by tyres which is taken as 20%.

Figure 2 Wheel topology optimisation model (see online version for colours)

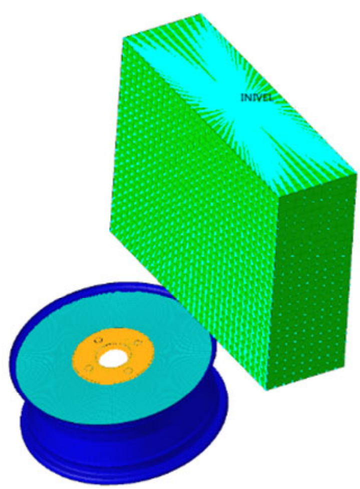

The specific topology optimisation process is shown in Figure 3: Passing the optimisation files from Radioss to OptiStruct (a subsidiary function of Hyperworks); Based on the initial starter and engine files, OptiStruct is used to establish the equivalent optimisation model; Based on the equivalent static multi-case, OptiStruct is used to optimise the topology, the starter and engine files are updated after optimisation, and the files are passed to Radioss for simulation; the Radioss simulation results are passed to OptiStruct for analysis to determine whether the convergence condition is reached. If convergence is achieved, the optimised model is output. If not, OptiStruct continues to optimise based on the updated simulation results, and the process is repeated until the final convergence.

Figure 3 Structural dynamic optimisation process

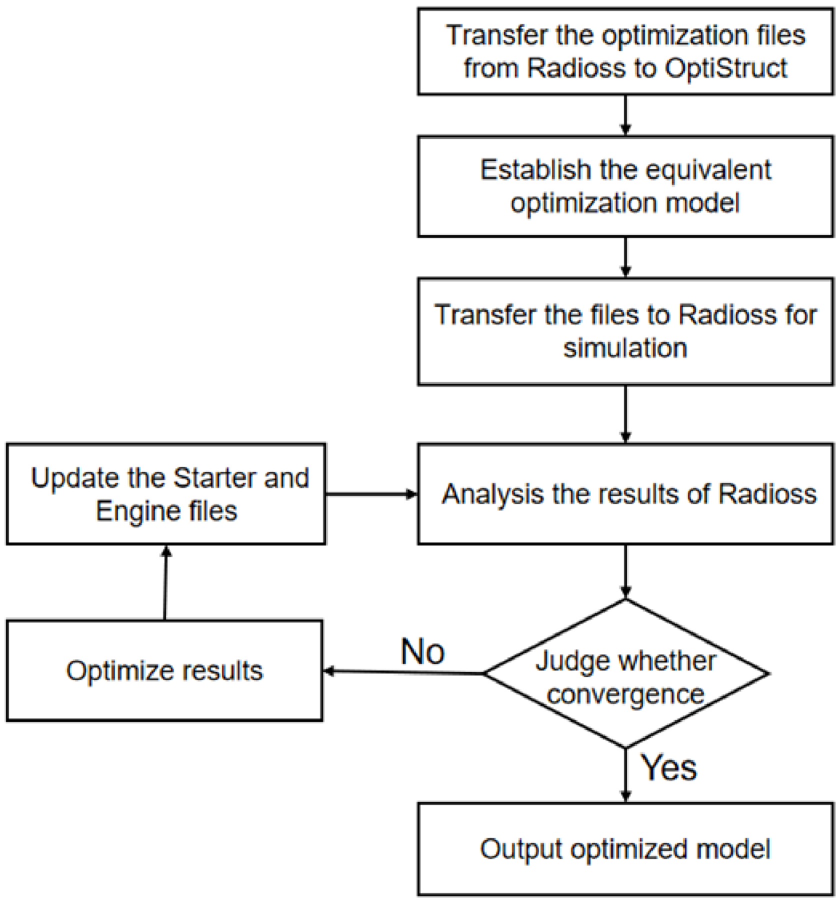

Because under impact load, the spokes of long fibre reinforced composite wheels designed earlier break through cracks, while other parts do not break. Therefore, spokes (except the mounting plane) are selected as the optimum area. Volume fraction not exceeding 40% of initial volume. To improve the stiffness of the wheels, the optimum objective is to minimise the maximum principal strain on the upper and lower surfaces of the spokes. The optimised wheel configuration is shown in Figure 4. To facilitate wheel fabrication and layer, the wheel configuration is simplified as shown in Figure 5.

Figure 4 Results of wheel topology optimisation (see online version for colours)

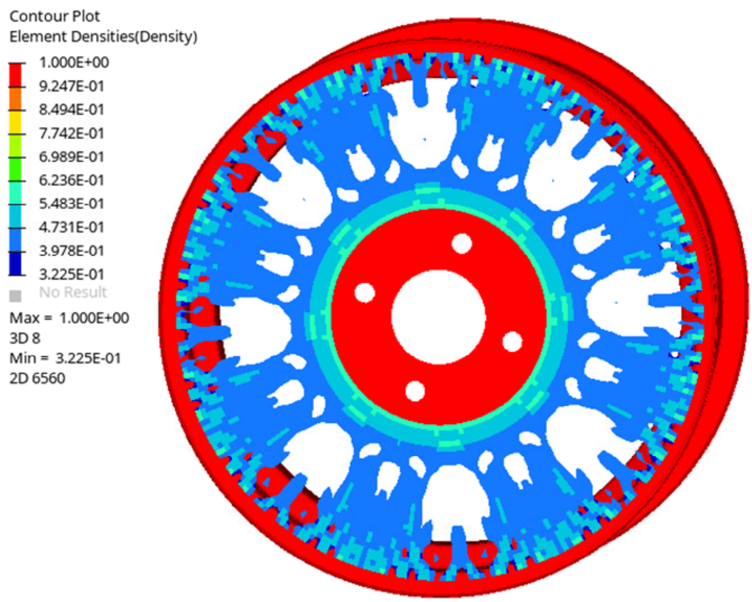

Figure 5 Simplified structure of wheel

2.3 Analysis of simulation results of 13-degree impact test on wheels

In the 13-degree impact test simulation, the isotropic model is used for the wheel. The wheel material is shown in Table 1. The basic properties and stress-strain curves of the material are calculated based on Digimat. Nominal strain should be transformed into real stress and strain, and plastic strain should be calculated to obtain the hardening curve of the material as shown in Figure 6.

Table 1 Composite material parameters

Name	*Parameter*
Matrix material	PA6
Reinforcement	CF
Mass fraction of CF	50%
Modulus	19.797GPa
Density	1.3929g/cm3
Poisson's ratio	0.2795

In order to improve the accuracy of simulation, the composite tyre model is used to model different parts of the tyre and assign corresponding material properties. At present, rubber is mainly used in tread, wall, shoulder and bead filler triangle of passenger tyre. In this paper, the Yeoh model is used to describe the mechanical properties of rubber (Li et al., 2021).

The ply and the belt ply in the tyre body are a composite of cord and rubber material. The cord of the tyre body is nylon and the cord of the ring and belt ply are steel wire. Furthermore, the 2-D and 3-D finite element models of the tyre are established. Figure 7. shows 2-D finite element models (Wan, 2017).

Figure 6 Material hardening characteristic curve

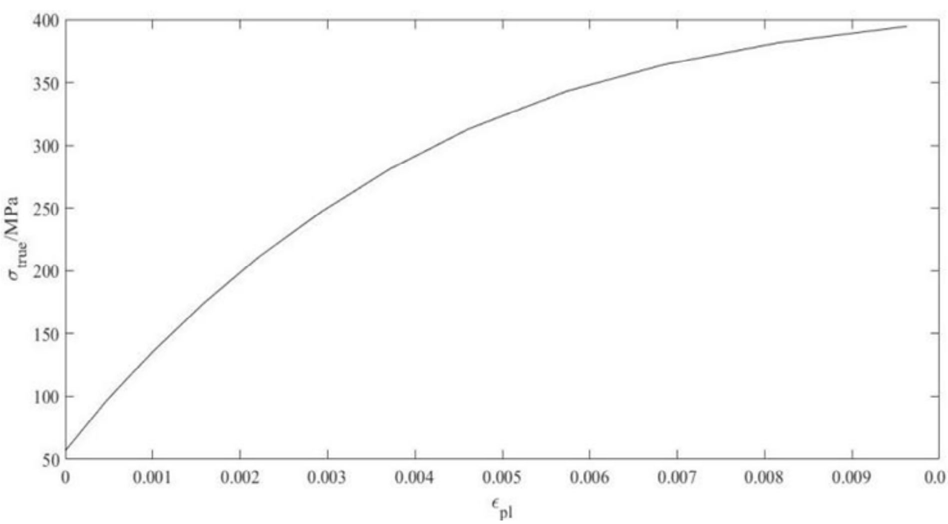

The impact test bench model and wheel model are established in ABAQUS for 13-degree impact test. Both the rim and the spokes are made of shell elements. The thickness of the rim is 6 mm, the thickness of the rim on the side is 12 mm, and the thickness of the spokes is 30 mm. Wheel weight is calculated as 4.61 kg. In the simulation, the tyre inflation pressure is set as 0.2 MPa. In order to improve the calculation efficiency, the drop height of the hammer is converted into the initial speed according to the law of conservation of energy. The calculation formula is:

$$v = \sqrt{2gH} \tag{3}$$

where v is the initial velocity of the hammer; g is gravity acceleration; H is the height at which the hammer falls.

The finite element simulation model of the 13-degree wheel impact test is shown in Figure 8.

Figure 7 2-D finite element model of tyre (see online version for colours)

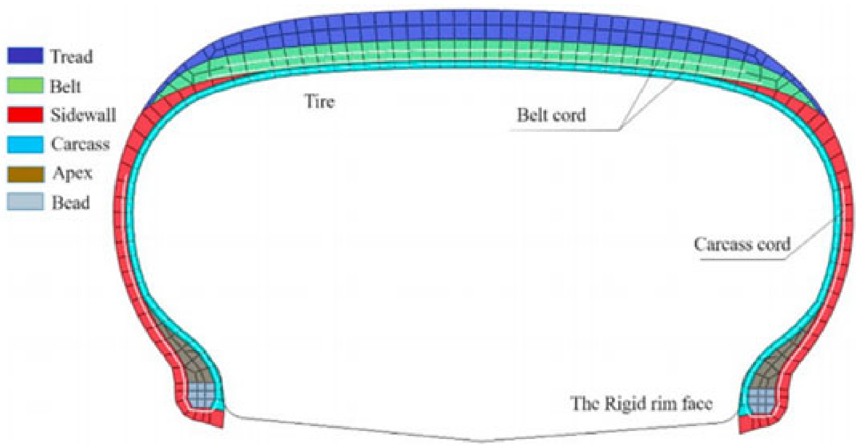

Figure 8 Finite element simulation model of wheel 13-degree impact test (see online version for colours)

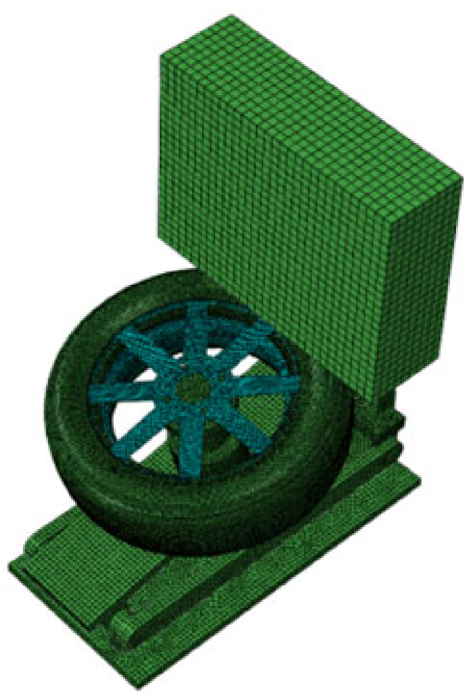

The impact test simulation shows that the maximum principal strain in the wheel is 3.159% and located at the base of the spoke, while the minimum principal strain is –3.298% and also located as the base of the spoke. But the fracture strain of the injection moulding wheel material is 3% (Xu, 2021), so both the maximum and minimum principal strains of the wheels exceed the fracture strain limits, and the long fibre-reinforced injection moulding wheel cannot pass the 13-degree impact test.

Figure 9 Cloud diagram of maximum and minimum principal strains of wheels (a) maximum strains (b) minimum strains (see online version for colours)

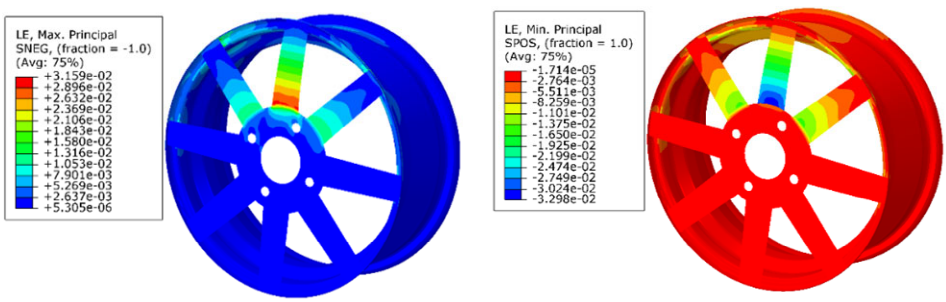

(a) (b)

By extracting the simulation results of five integration points (shown in Figure 10)on the section of spoke root position, the curve of maximum principal strain with time can be obtained, as shown in Figure 11, which shows that the deformation characteristics at the spoke root are similar to those of the beam under bending moment. The strain on the upper and lower surfaces is maximum, and the deformation in the middle is small. Therefore, based on the beam bending model, the stiffness matching design of the spoke section is carried out by using the laminated reinforced spokes.

Figure 10 The positions of the five integral points on the section

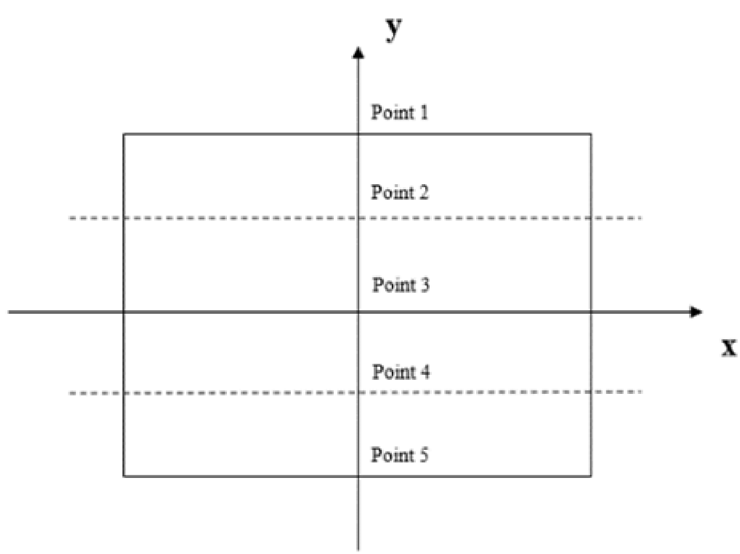

Figure 11 Maximum principal strain curve at spoke section point (see online version for colours)

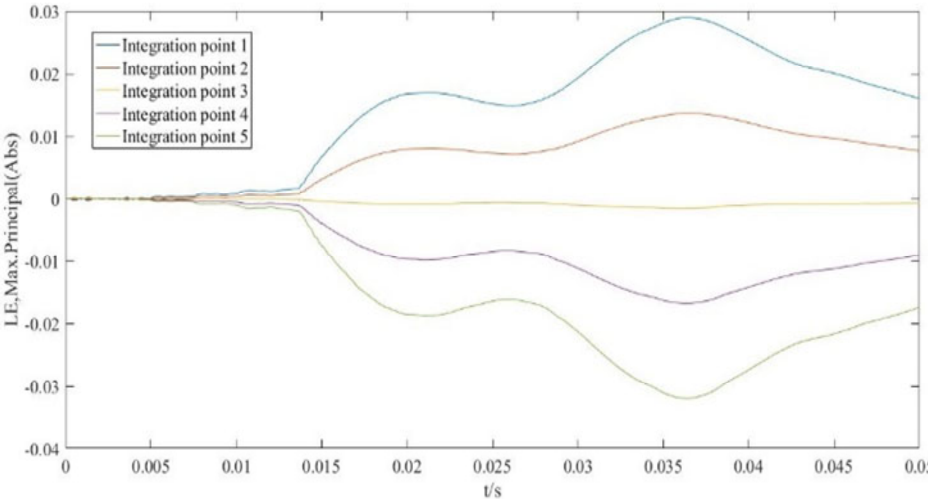

3 Design of spoke section stiffness matching

From above simulation results, the spoke root fracture occurs under impact load, so it needs to be strengthened. Considering the impact resistance and weight of the spokes, layering may be used to strengthen the spoke. Based on the beam bending model, the equal strength theory is used to determine the position of the ply and the material proportion of the spoke section.

3.1 Simplified spoke force model of hybrid structure under impact condition

Under the impact load, the simplified model of the forces acting on the spoke section is shown in Figure 12.

Figure 12 Simplified spoke force model with layer outside spoke

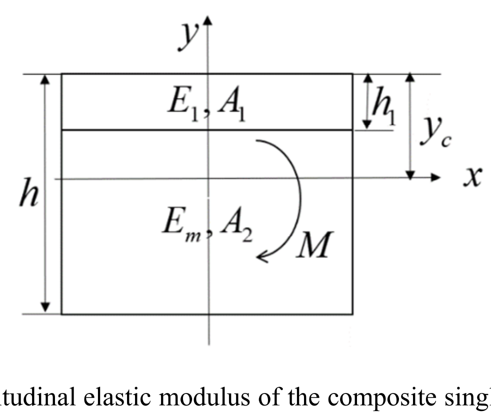

where, $E1$ is the longitudinal elastic modulus of the composite single-layer; A_1 is the area occupied by the layer; E_m denotes the elastic modulus of injection moulding; A_2

represents the area occupied by injection moulding; X-axis is the neutral axis; y_c indicates the distance from the neutral axis to the upper surface; h is the thickness of the section; h_1 is the total thickness of the pavement.

According to the results of impact tests, the bending moment on the section is the main factor affecting the spoke strain, so the effect of shear is neglected when simplifying the model. At the same time, the maximum strain is located on the upper and lower surface of the spoke. At the surface of the spoke, the material is in unidirectional tension and compression. When the ply is on the surface of the spoke and the thickness of the ply is small relative to the total thickness of the spoke section, the composite monolayer can be considered to be in plane stress state. The composite single-layer plate used in this paper is CF/PA6.

3.2 Feasibility analysis of laying layer outside the spoke

In this paper, Tsai-Wu criterion is adopted as the failure criterion of composite single-layer, as shown in equation (4):

$$F_1\sigma_1 + F_2\sigma_2 + F_{11}\sigma_1^2 + F_{22}\sigma_2^2 + F_{66}\sigma_6^2 + 2F_{12}\sigma_1\sigma_2 = 1 \tag{4}$$

where $F_1 = \frac{1}{X_t} - \frac{1}{X_c}$, $F2 = \frac{1}{Y_t} - \frac{1}{Y_c}$, $F_{11} = \frac{1}{X_t\ X_c}$, $F_{22} = \frac{1}{Y_tY_c}$, $F_{66} = \frac{1}{S^2}$, $F_{12} = -0.25$. X_t and X_c are the strength of longitudinal tensile and compressive; Y_t and Y_c are the strength of longitudinal tensile and compressive.

The maximum strain of the wheel is located at the upper and lower surfaces of the spokes. On the spoke surface, the material is in a unidirectional tension-compression state. Then, when the ply is on the spoke surface and the thickness of the ply is very small relative to the total thickness of the spoke section, the composite single-layer can be considered to be in the plane stress state. The stress-strain relationship is shown in equation (5).

$$\begin{pmatrix} \varepsilon_1 \\ \varepsilon_2 \\ \gamma_{12} \end{pmatrix} = \begin{pmatrix} S_{11} & S_{12} & 0 \\ S_{12} & S_{22} & 0 \\ 0 & 0 & S_{66} \end{pmatrix} \begin{pmatrix} \sigma_1 \\ \sigma_2 \\ \tau_{12} \end{pmatrix} \tag{5}$$

where $S_{11} = \frac{1}{E_1}$, $S_{12} = \frac{v_{12}}{E_2}$, $S_{66} = \frac{1}{G_{12}}$, E_1 is longitudinal elastic modulus; E_2 is transverse modulus of elasticity; G_{12} is the in-plane shear modulus. υ_{12} is in-plane Poisson ratio; S_{12} is in-plane shear strength.

On the inner and outer surfaces of the spokes, the single-layer plates are subjected to tensile and compressive stresses respectively, and are in uniaxial tension and compression. Therefore $\sigma_2 = \tau_{12} = 0$, Tsai-Wu failure criterion can be simplified to equation (6)

$$F_1\sigma_1 + F_{11}\sigma_1^2 = 1 \tag{6}$$

When the single-layer plate fails, the longitudinal tensile strain and the compressive strain are shown in equation (7) and equation (8) respectively.

$$\varepsilon_{tu} = \frac{X_t}{E_1} = 1.929 \times 10^{-2} \tag{7}$$

$$\varepsilon_{cu} = -\frac{X_c}{E_1} = -0.491n?10^{-2} \tag{8}$$

where ε_{tu} and ε_{cu} are the fracture strains of the single-layer plate under longitudinal uniaxial tension and compression respectively.

In order to make full use of the material, the spoke section needs to be designed according to the theory of equal strength. When the maximum strain of the injection moulding reaches the failure strain, the ply also fails and both fail at the same time. Under the action of bending moment, the strain on the section is linearly distributed along the height.

$$\frac{\varepsilon_{tu}}{\varepsilon_m} = \frac{y_c}{h - y_c} \tag{9}$$

where ε_m is 3% of the fracture strain of the injection moulding part.

Assuming that the property of the ply and the injection material is linear elastic, according to Hooke's law, the torque balance at the point from the neutral axis y_c can be obtained:

$$E_1 S_{X_1} + E_m S_{X_m} = 0 \tag{10}$$

where E_m denotes the elastic modulus of the injection moulding; S_{X_1} is the static moment of the paving part with respect to the neutral axis X; S_{X_m} represents the static moment of the injection part with respect to the neutral axis X.

$$S_{X_1} = \int_{A_1} y dA = h_1 b \left(y_c - \frac{h_1}{2} \right) \tag{11}$$

$$S_{X_m} = \int_{A_2} y dA = \frac{b}{2}\left[2 y_c (h - h_1) + h_1^2 - h^2 \right] \tag{12}$$

where b is the section width.

By combining equations (10)-(12), equation (13) can be obtained:

$$y_c = \frac{E_1 h_1^2 + E_m \left(h^2 - h_1^2 \right)}{2\left[E_1 h_1 + E_m (h - h_1) \right]} \tag{13}$$

The layer thickness h_1 = 1.95 mm or h_1 = 21.53 mm is calculated by combining equations (9) and (13). Tensile fracture occurs when the layer thickness is 21.53 mm. When the thickness of the layer is 21.53 mm and the injection moulding breaks in tension, the maximum compression strain is $\varepsilon_{cmax} = \dfrac{y_c}{h - y_c} \varepsilon_{tu} = -1.609 \times 10^{-2}$. However, the fracture strain of the single-layer plate under longitudinal unidirectional compression is 0.491×10^{-2}. Because the compression failure of the layer occurs earlier than that of the single-layer plate, the thickness of the layer cannot be selected. The thickness of the layer and the single-layer plate are 1.95 mm and 0.15 mm respectively, and the total number of layers is 13.

3.3 Feasibility analysis of laying layer inside the spoke

When the layer is located at the inside of the spoke, the sectional stress model is shown in Figure 13. Since the injection part is located outside the spoke, the failure of the injection part is caused by tensile fracture while the failure of the laminate is mainly caused by compressive fracture.

Figure 13 Simplified spoke force model with layer inside spoke

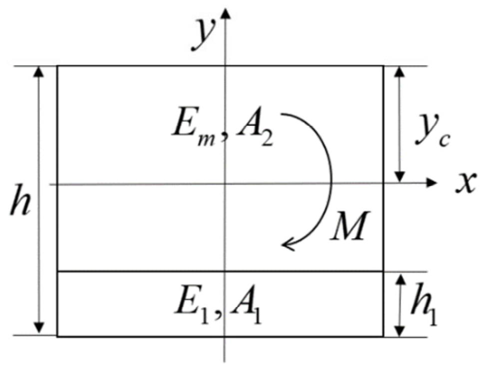

When both the layer and the injection moulding are destroyed at the same time, equation (14) can be obtained according to equation (8).

$$\frac{\varepsilon_m}{\varepsilon_{cu}} = \frac{y_c}{y_c - h} \tag{14}$$

The distance from the neutral axis to the outer surface of the spoke is:

$$y_c = \frac{\varepsilon_m}{\varepsilon_m - \varepsilon_{cu}} h \tag{15}$$

The static moments of the layer and injection parts to the neutral axis are:

$$S_{X_1} = \int_{A_1} ydA = \frac{h_1 b}{2}[h_1 + 2(y_c - h)] \tag{16}$$

$$S_{X_m} = \int_{A_2} ydA = \frac{b}{2}(h - h_1)(2y_c + h_1 - h) \tag{17}$$

By combining equations (10), (16) and (17), the value of y_c can be obtained:

$$y_c = \frac{E_1 h_1 (2h - h_1) + E_m (h^2 - h_1^2)}{2[E_1 h_1 + E_m (h - h_1)]} \tag{18}$$

Based on equations (15) and (18), the thickness h_1 of the layer cannot be determined. Therefore, when the spokes are located at the inner side of the layer, the layer and the injection moulding parts cannot be damaged at the same time which results in that the material cannot be used optimally. To achieve equal strength design, the layer should be located on the outside of the spoke with the thickness of 1.95 mm, consisting of 13 layers.

3.4 The 13-degree impact test simulation and structural improvement of compression/injected composite wheel

The direction of layer is shown in Figure 14. Direction 1 (blue) is along the centre line of the spoke, direction 2 (yellow) is perpendicular to direction 1, and direction N (red) is the direction of stacking. The 13-degree impact test simulation is carried out for the initial wheel of composite structure.

Figure 14 Lamination direction of composite material (see online version for colours)

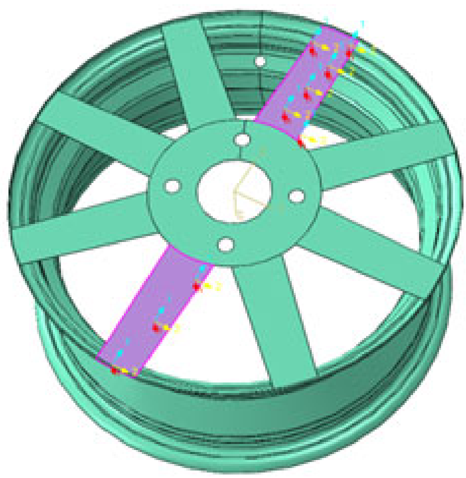

Figure 15 Distribution cloud of failure factor TSAIW (see online version for colours)

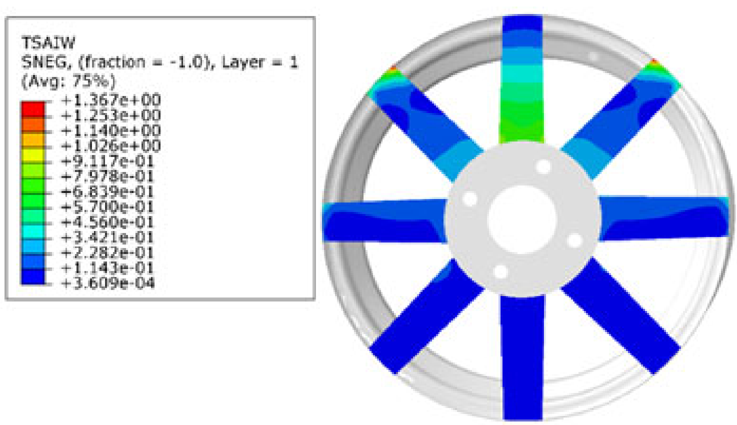

Figure 16 Distribution of maximum principal strain on spoke surface under impact load (see online version for colours)

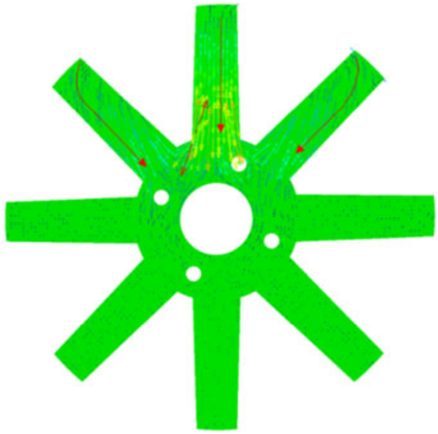

The failure factor TSAIW of single-ply plates is defined as equation (19). When TSAIW is greater than 1, the single-ply plate fails. The TSAIW distribution of single-layer plate under impact load is shown in Figure 15.

$$F_1\sigma_1 + F_2\sigma_2 + F_{11}\sigma_1^2 + F_2\sigma\,?_2^2 + F_{66}\sigma_6^2 + 2F_{12}\sigma_1\sigma_2 = TSAIW \quad (19)$$

From Figure 15, the maximum failure factor TSAIW of the single-layer plate is 1.367, which exceeds 1, and the spoke is destroyed close to the rim. The direction distribution of the maximum principal strain of the spoke is extracted for analysis. During the impact, the energy is transferred along the curve in Figure 16. Near the rim, the angle between the direction of the maximum principal strain and the fibre is large.

Figure 17 TSAIW distribution cloud of initial wheel with hybrid structure (see online version for colours)

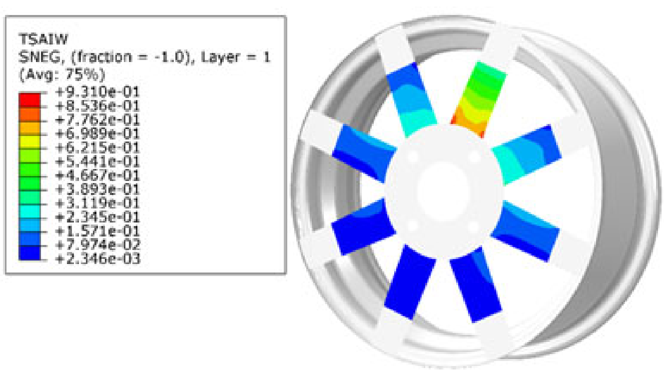

Due to the poor lateral mechanical properties of the single-layer, the layer should not extend to the rim in order to achieve the excellent longitudinal tensile properties of the single-layer. After modifying the layering, the impact test simulation is conducted again. The results are shown in Figures 17–18. The composite wheel with the compression/injection structure can pass the 13-degree impact test.

Figure 18 Cloud view of minimum principal strain distribution for hybrid wheels (see online version for colours)

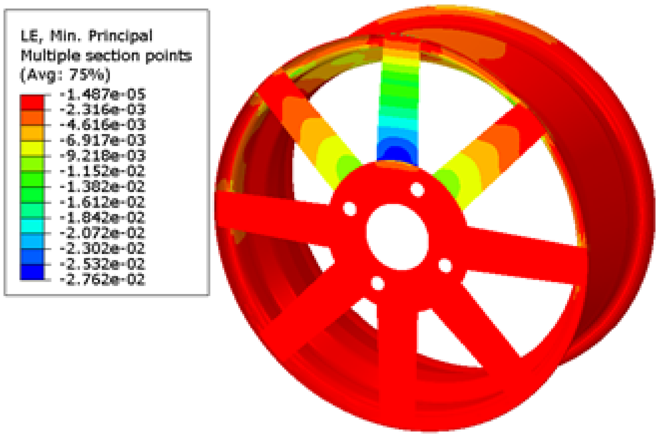

4 Parameter optimisation of compression /injection moulding composite wheel

4.1 The 13-degree impact test simulation and structural improvement of compression/injection moulding composite wheel

A great time cost is required to simulate the wheel 13-degree impact test . In order to save the calculation time, the energy reduction ratio of wheel with mixed compression/injection structure may be obtained by calculating the energy absorbed during the impact process. Then the tyre structure may be removed from the wheel impact simulation model, so the purpose of saving calculation cost may be achieved when optimising the parameters of the composite wheel.

Figure 19 Energy absorbed by tyre during impact

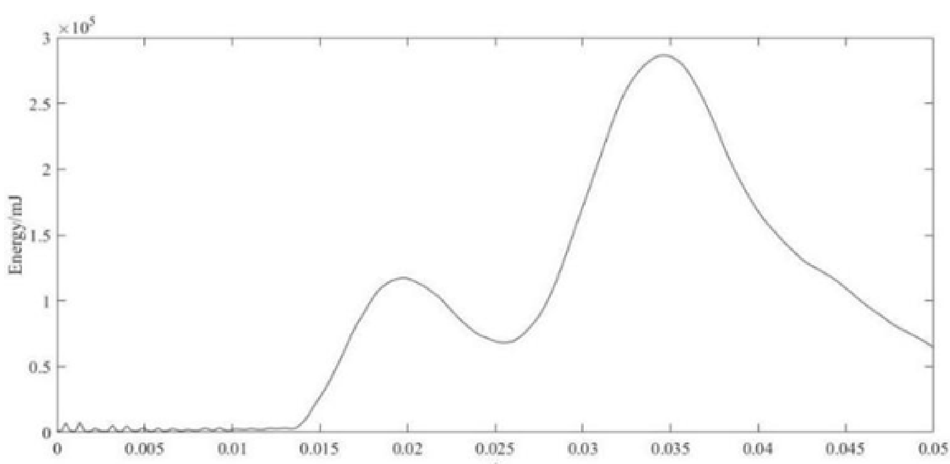

Figure 20 Finite element simulation model of 13-degree wheel impact test without tyre (see online version for colours)

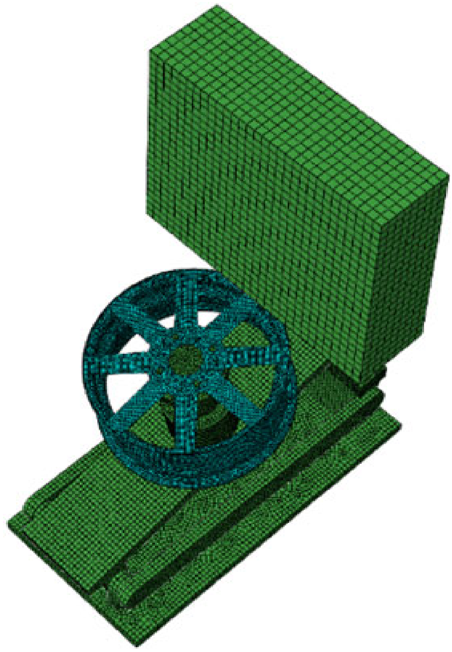

At present, it is generally assumed that the tyre absorbs 20% of the energy during the impact process. However, the wheel in literature is made of aluminium and inconsistent with the wheel material used in this paper (Shang et al., 2005), so it is necessary to study the energy absorbed by tyres in the impact process of hybrid composite wheels. The maximum of the total tyre energy during impact is extracted and the ratio of the total tyre energy to the total system energy is taken as the proportion of energy reduction as shown in equation (20):

$$\eta = \frac{E_{tire}}{E_{TOTAL}} = \frac{IE_{tire} + KE_{tire} + VD_{tire}}{E_{TOTAL}} \tag{20}$$

where η is the energy reduction ratio; E_{tire} denotes the total energy of the tyre; IE_{tire} indicates the internal energy of the tyre; KE_{tire} represents the kinetic energy of the tyre; VD_{tire} is the tyre viscous dissipation energy; E_{TOTAL} is the total energy of the system.

The change of the total tyre energy during the impact process is shown in Figure 19. The energy reduction ratio of the tyre in this paper during the impact process is calculated to be 12.3%.

In order to verify the rationality of the energy reduction ratio, the 13-degree impact test simulation model of a wheel without tyres is established, and the 13-degree impact test simulation is carried out as shown in Figure 20. The TSAIW of the single-layer board is shown in Figure 21, and the minimum principal strain of the injection moulding part is shown in Figure 22.

Figure 21 TSAIW cloud diagram of tyre model without failure factor (see online version for colours)

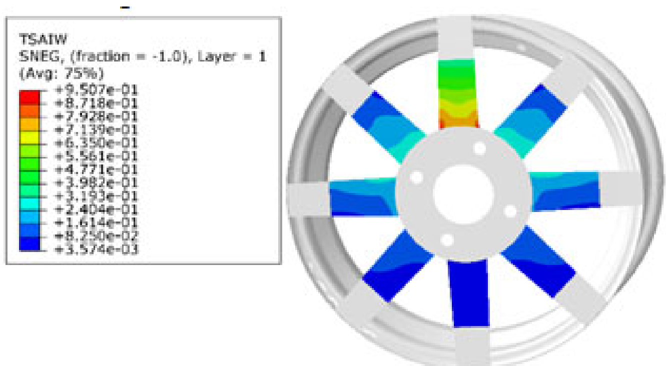

Figure 22 Minimum principal strain cloud for injection moulding without tyre model (see online version for colours)

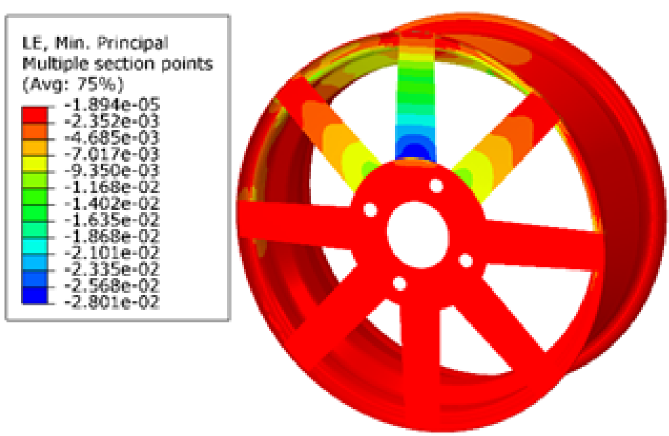

As shown in Table 2, the TSAIW and minimum principal strain of the injection moulding part of the single-layer board with and without the tyre model are compared. The relative error of the failure factor TSAIW is 2.12%, and the relative error of the minimum principal strain is 1.41%. The simulation results of the model with tyres and the model without tyres are close, which shows that the energy reduction ratio of 12.3% is reasonable. Therefore, through the introduction of the energy reduction ratio, the deletion of tyre model in the model used for subsequent simulation is feasible.

Table 2 Simulation results of the model with and without tyres

	TSAIW	*LE, min. principal*
Model with tyres	0.9310	-2.762×10^{-2}
Model without tyres	0.9507	-2.801×10^{-2}
Relative error	2.12%	1.41%

Figure 23 Spoke design parameters

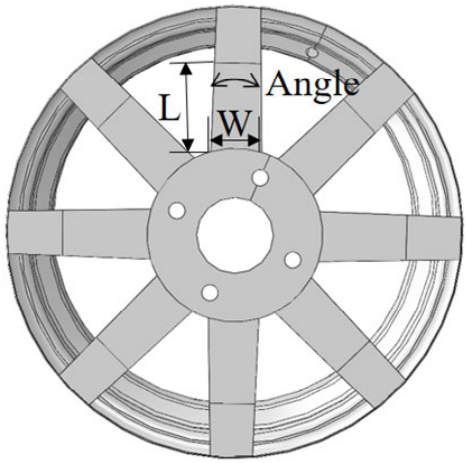

4.2 Wheel parameter optimisation based on multi-island genetic algorithm

To further achieve wheel lightweight, the parameters of the wheels are optimised. Rim width B, layering length L, width W, Angle, thickness T and rim width B are selected as wheel optimisation parameters as shown in Figure 23. The experimental design is carried out, which uses the optimised Latin hypercube sampling to select 50 groups of sample points.

According to the simulation results of the sample points, the RBF model is used to construct an approximate model. In order to verify the accuracy of response surface, eight groups of test points are selected for response surface evaluation. The R2 of each response quantity (shown in Table 4) is greater than 0.9, indicating that the approximate model is reliable. The approximate model is optimised with the aim of minimising the wheel mass. The constraints are that the failure factor TSAIW of the single-ply plate is less than 1, and the minimum and maximum principal strains of the injection moulding parts do not exceed 3% of the material fracture strain. The multi-island genetic algorithm is used for the optimisation algorithm. The values of the optimised parameters are shown in Table 3.

Table 3 Results of parameter optimisation

Parameter	*Angle/°*	*B/mm*	*L/mm*	*T/mm*	*W/mm*
Optimised results	14	11.4	65.26	1.65	43.52

Table 4 R2 value for each response quantity

Response	*m*	*TSAIW*	*strain-min*	*strain-max*
R2	0.99991	0.96115	0.99618	0.99169

Figure 24 Minimum and maximum principal strain contours of injection moulding parts (a) maximum strains (b) minimum strains (see online version for colours)

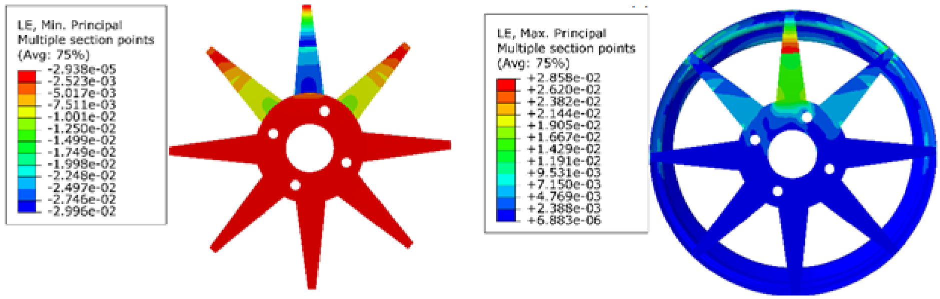

(a) (b)

Figure 25 TSAIW cloud diagram of single-layer board (see online version for colours)

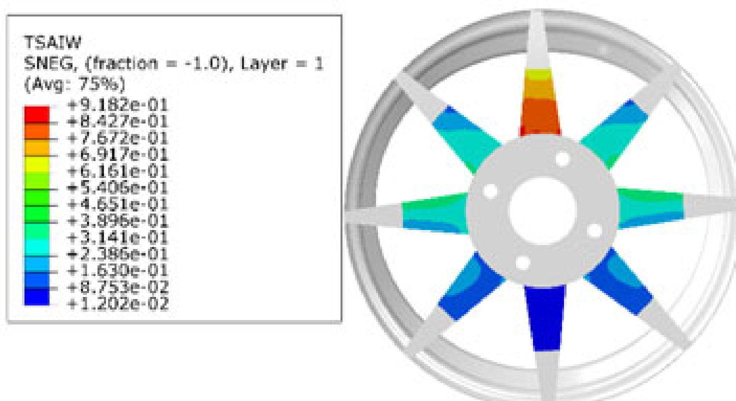

After optimisation, the total thickness of the layers is 1.65 mm, the thickness of the single-layer board is 0.15mm, and the number of layers is calculated as 11. The 13-degree impact test simulation of the optimised wheel is carried out. The minimum and maximum principal strains of the injection moulding parts are shown in Figure 24, and the failure factor TSAIW of the single-layer board is shown in Figure 25. The actual simulation results of each response quantity and the predicted results of the approximate model are shown in Table 5.

Table 5 Predicted and simulated values of each response quantity

Parameter	*m/kg*	*TSAIW*	*Strain-min/×10^–2^*	*Strain-max/×10^–2^*
Simulation value	3.92057	0.9182	2.858	2.996
Predictive value	3.88188	0.9410	2.927	2.967
Error	1.0%	–2.42%	–2.36%	0.98%

The mass of optimised wheel is calculated as 3.921 kg, so a weight reduction of 0.689 kg and a weight loss rate of 14.9% are obtained relative to 4.61 kg before optimisation. And the weight of the same type of aluminium wheel is 6.84 kg, so a weight reduction of 2.919 kg and a weight loss rate of 42.7% are also achieved.

5 Conclusions

In this paper, the topology optimisation of the wheel is performed for the 13-degree impact dynamic condition, and the wheel configuration with better impact resistance is obtained. Based on the beam bending model, the stiffness matching design of spoke section is carried out, and the ratio of the ply position to the thickness of different composites is obtained. The final structure of the wheel is obtained by parameter optimisation of the wheel. The main conclusions are as follows:

1 Continuous fibre composite material used in the spoke may improve the impact resistance of the spoke to pass the 13-degree impact test.

2 Considering the type of material selected in this paper, when the continuous fibre reinforced composite material layup structure is located on the outer side of the wheel spoke, the equal strength design of the two materials in the wheel spoke can be realised.

3 For the compression/injection moulding composite wheel designed in this paper, the energy reduction ratio of the tyre of 12.3% is reasonable rather than the commonly used 20%.

4 The optimised wheels can pass 13-degree impact test, and has a better lightweight effect. Its weight loss rate reaches 14.9% relative the unoptimised wheel, and 42.7% compared with the same type of aluminium wheel.

Acknowledgements

This work was financially supported by the National Natural Science Foundation of China (No. 52275232 and No. 51875025).

References

Benedyk, J.C. (2000) ‘Light metals in automotive applications’, *Light Metal Age*, Vol. 58, Nos. 9–10, pp.34–35.

Bian, W.F. et al. (2008) ‘Intensity analysis and layer design for automobile wheel made of complex material’, *Journal of Mechanical Strength*, Vol. 30, No. 2, pp.315–318.

Chai, W. et al. (2018) ‘Research on simulation of the bending fatigue test of automotive wheel made of long glass fibre reinforced thermoplastic considering anisotropic property’, *Advances in Engineering Software*, Vol. 116, pp.1–8.

Chang, S.W. et al. (2010) ‘A simulation analysis on the impact test of composite wheel’, *Journal of Automotive Engineering*, Vol. 32, No. 1, pp.65–68.

Chen, S.J. (2011) ‘Application of advanced composites on automotive filed’, *Hi-Tech Fibre and Application*, Vol. 36, No. 1, pp.11–17.

Czerwinski, F. (2021) ‘Current Trends in automotive lightweighting strategies and materials’, *Materials*, Vol. 14, No. 21, p.6631.

Grace (2014) ‘SABIC and Kringlan jointly develop the world’s first thermoplastic carbon composite wheel (in Chinese)’, *Shanghai Chemical Industry*, Vol. 39, No. 6, p.42.

Hu, D. et al. (2019) 'Research on simulation method of impact resistance of composite wheels made of long glass fibre reinforced thermoplastic introducing anisotropic property', *Composite Structures*, Vol. 223, DOI:10.1016/ j.compstruct. 2019.110965.

Hua, Z. (2015) 'Ford's world's first mass-produced carbon fibre wheel pushes the application of lightweight materials (in Chinese)', *Hi-Tech Fibre and Application*, Vol. 40, No. 5, pp.64–65.

Kang, B.S. et al. (2001) 'Structural optimization under equivalent static loads transformed from dynamic loads based on displacement', *Computers and Structures,* Vol. 79, No. 2, pp.145–154.

Li, B.P. et al. (2016) 'Research on moulding process and property of automobile composite wheel, development and application of materials', *Development and Application of Materials*, Vol. 31, No. 2, pp.37–41.

Li, Y.X. et al. (2021) 'Nonlinear dynamic topology optimization on equivalent static loads method', *Chinese Journal of Computational Mechanics*, Vol. 38, No. 3, pp.377–383.

Miller, W. et al. (2000) 'Recent development in aluminium alloys for the automotive industry', *Materials Science and Engineering A*, Vol. 280, No. 1, pp.37–49.

Shang, R. et al. (2005) 'Wheel impact performance with consideration of material inhomogeneity and a simplified approach for modeling', *International Journal of Crashworthiness*, Vol. 10, No. 2, pp.137–150.

Wan, X.F. (2017) *Research on Tire-wheel Load Transfer Characteristic and Its Application in the Simulation of Wheel Strength Test*, Beijing: Beijing University of Aeronautics and Astronautics.

Wan, X.F. et al. (2015) 'Influence of material anisotropy on long glass fibre reinforced thermoplastics composite wheel: dynamic impact simulation', *ASME International Mechanical Engineering Congress and Exposition, Proceedings (IMECE)*, Vol. 14, DOI: 10.1115/IMECE2015-50725.

Xu, W.C. (2021) *Research on Structure-Connection-Performance Integration Multi-Objective Optimization Design Method of Multi-material Assembled Wheel*, Jilin University, DOI:10.27162/d.cnki.gjlin.2021.007516.